AIAA JOURNAL
Vol. 40, No. 3, March 2002

Aeroacoustics of Wall-Bounded Turbulent Flows

Z. W. Hu,* C. L. Morfey,† and N. D. Sandham‡
University of Southampton, Southampton, England SO17 1BJ, United Kingdom

Direct numerical simulations of turbulent plane Poiseuille and Couette flow are used to study fluctuating wall pressure and shear stress. For both flows the wave-number–frequency spectra are found to be nonzero in the limit of zero wave number, which has significant implications for theoretical work. Peaks in the spectra are consistent with convective phenomena, and typical convection speeds are derived for both cases. The sensitivity of the results to Reynolds number and numerical parameters is discussed.

Nomenclature

$C(t)$	=	arbitrary reference pressure
E	=	mathematical expectation
f	=	frequency
h^*	=	channel half-width
i	=	$\sqrt{-1}$
$\boldsymbol{k}$	=	wave-number vector, $\boldsymbol{k} = (k_x, k_y) = (k_x^*, k_y^*)h^*$; $(k_{x_l}, k_{y_m}) = (2\pi l/L_x, 2\pi m/L_y)$, with l and m being streamwise and spanwise mode numbers, $0 \le l \le N_x/2$; $-N_y/2 \le m \le N_y/2$
L_x, L_y	=	computational box lengths
L_{ref}^*	=	reference length
N	=	number of time samples
N_x, N_y, N_z	=	number of grid points
p	=	pressure relative to background value $C - \Lambda x$
Re	=	Reynolds number
S_p	=	wall pressure spectral density
S_τ	=	wall shear-stress spectral density
T	=	total record length
t	=	time
U_{ref}^*	=	reference velocity
u_i	=	velocity components ($i = 1, 2, 3$), also (u, v, w)
u_w	=	wall velocity
u_τ	=	friction velocity
x_i	=	coordinates ($i = 1, 2, 3$), also (x, y, z)
x_i, y_j, z_k	=	grid coordinates, ($1 \le i \le N_x$, $1 \le j \le N_y$ and $1 \le k \le N_z$)
Δt	=	sampling time interval
ϵ_{ijk}	=	permutation tensor
Λ^*	=	wall shear stress averaged over both walls/h^*
ν^*	=	kinematic viscosity of the fluid
Π	=	modified pressure, $\Pi = p + u_i u_i/2$
ρ^*	=	density
τ_{ij}	=	viscous stress, $\tau_{ij} = \nu(\partial u_i/\partial x_j + \partial u_j/\partial x_i)$
ω_i	=	vorticity; $\omega_i = \epsilon_{ijk}\partial u_k/\partial x_j$

Superscripts

$*$	=	dimensional quantity
$\star$	=	complex conjugate
$'$	=	fluctuation quantity
$\tilde{}$	=	quantity in Fourier space
$-$	=	statistical average
$+$	=	wall units

Received 29 March 2001; presented as Paper 2001-2172 at the AIAA/CEAS 7th Aeroacoustics Conference, Maastricht, The Netherlands, 28–30 May 2001; revision received 6 August 2001; accepted for publication 7 August 2001.

*Research Fellow, Aeronautics and Astronautics, School of Engineering Sciences.
†Professor, Fluid Dynamics and Acoustics Group, ISVR.
‡Professor, Aeronautics and Astronautics, School of Engineering Sciences. Member AIAA.

I. Introduction

PLANE channel flow is a geometrically simple problem that has played an important role in understanding the mechanics of wall-bounded turbulence. Experiments have been able to provide some useful data on plane channel flows: examples include Hussain and Reynolds[1] for plane Poiseuille flow and Tillmark and Alfredsson[2] for plane Couette flow. However, a lack of accurate techniques for measuring velocity fluctuations simultaneously in all directions, and for measuring velocity–pressure fluctuation correlations, severely limits the information available.

On the other hand, direct numerical simulation (DNS) has proved to be a reliable tool for turbulence investigation. With the help of supercomputers DNS can now tackle turbulent fluid flows over a range of Reynolds numbers, and it has been widely used in the study of turbulence mechanisms. DNS of plane Poiseuille flow[3–5] has been able to provide high-order statistical moments of velocity and pressure and also energy budgets. DNS studies have additionally been published[6–8] for plane Couette flow. A difference between the two types of flow is that in Couette flow very long large-scale structures exist in the core region (midway between the walls).

Despite these and other investigations, few simulations of plane channel flow have been carried out in a computational domain large enough to allow both the streamwise and spanwise two-point correlations to drop satisfactorily to zero. Furthermore, in low-Mach-number aeroacoustics there is particular interest in the low wave-number structure because of its ability to excite sound and structural vibration. To obtain low-wave-number results, the simulation domain needs to be large.

Existing studies on the low-wave-number behavior of turbulent wall pressure and shear stress are contradictory. Kraichnan[9] and Phillips[10] suggested on theoretical grounds that the wave-number–frequency spectrum of wall pressure $S_p(\boldsymbol{k}, f)$ tends to zero in incompressible flow as $\boldsymbol{k} \to 0$, provided $f \neq 0$ (Kraichnan–Phillips theorem). Chase[11–13] later concluded that although the Kraichnan–Phillips theorem holds for inviscid flow, in real viscous flow the (k_x, k_y) wave-number spectra of wall pressure and shear stress approach nonvanishing limits when the no-slip boundary condition is applied. Measurements of turbulent boundary-layer wall-pressure fluctuations at low Mach number by Herbert et al.[14] have shown a finite k_x spectrum at low wave numbers. However, Howe[15] has claimed that even for viscous flow the incompressible (k_x, k_y) wall-pressure spectrum should tend to zero at zero wave number for all nonzero frequencies.

In further studies of wall shear stress, Chase[16,17] developed a semi-empirical spectral model for the nonvanishing zero wave-number spectrum of shear stress on a single plane wall and compared the model with experiment. However, Howe[18–20] argued that the wall shear stress modifies sound propagation, but does not generate any sound radiation. Its wave-number–frequency spectrum was predicted to behave similarly to the wall pressure.[13,19,20]

In the present study turbulent plane Poiseuille flow and Couette flow are simulated directly for incompressible flow in very large computational domains. Results are compared with previous work, and DNS databases from the simulation are then used to study the low-wave-number behavior of the wave-number–frequency spectrum, both for turbulent wall pressure and wall shear stress.

II. DNS of Incompressible Plane Channel Flow

The governing continuity and momentum equations of incompressible turbulent flow are nondimensionalized with the reference length L^*_{ref} chosen as the channel half-width h^*. The reference velocity U^*_{ref} is the friction velocity u^*_τ for Poiseuille flow and the wall velocity u^*_w for Couette flow. (Both the upper and the lower wall move, with velocity u^*_w and $-u^*_w$, respectively.) The steady background pressure field is subtracted out, along with a time-dependent reference pressure, to give the relative pressure p^*. Nondimensional quantities are then defined as

$$u_i = u_i^* \big/ U^*_{\text{ref}}, \qquad x_i = x_i^* \big/ h^*, \qquad p = p^* \big/ \left(\rho^* U^{*2}_{\text{ref}}\right)$$

$$t = t^* U^*_{\text{ref}} \big/ h^*$$

The nondimensional continuity equation and rotation form of the momentum equation become[21]

$$\frac{\partial u_j}{\partial x_j} = 0 \tag{1}$$

$$\frac{\partial u_i}{\partial t} = \epsilon_{ijk} u_j \omega_k + \delta_{1i}\Lambda - \frac{\partial \Pi}{\partial x_i} + \frac{1}{Re}\frac{\partial^2 u_i}{\partial x_j \partial x_j} \tag{2}$$

where Reynolds number is $Re = U^*_{\text{ref}} h^*/\nu^*$, equal to $Re_\tau = u^*_\tau h^*/\nu^*$ for Poiseuille flow, and $Re_w = u^*_w h^*/\nu^*$ for Couette flow. Λ is the nondimensional mean pressure gradient, equal to one for Poiseuille flow and zero for Couette flow.

It is convenient for the DNS description to replace the x_i notation by (x, y, z) with corresponding velocity components (u, v, w). The coordinates are x in the streamwise direction, y in the spanwise direction, and z in the wall-normal direction with the channel walls at $z = \pm 1$.

Following the spectral method of Kleiser and Schumann,[22] Fourier discretization is used for the two periodic directions, namely, streamwise and spanwise. A two-dimensional Fourier transformation from real to wave space is accomplished by a streamwise real-to-complex Fourier transformation, followed by a complex-to-complex Fourier transformation in the spanwise direction. A real quantity $q(x, y)$ is transformed to wave space $\tilde{q}(k_x, k_y)$ by the two successive discrete Fourier operations:

$$\tilde{q}(k_{x_l}, y_j) = \frac{1}{N_x}\sum_{i=0}^{N_x-1} q(x_i, y_j)\exp\left(\frac{-\mathrm{i}2\pi li}{N_x}\right) \tag{3}$$

$$\tilde{q}(k_{x_l}, k_{y_m}) = \frac{1}{N_y}\sum_{j=0}^{N_y-1} \tilde{q}(k_{x_l}, y_j)\exp\left(\frac{-\mathrm{i}2\pi mj}{N_y}\right) \tag{4}$$

The two-dimensional backward transformation is done with a spanwise complex-to-complex transformation, followed by a streamwise complex-to-real transformation:

$$\tilde{q}(k_{x_l}, y_j) = \sum_{m=-N_y/2}^{N_y/2} \tilde{q}(k_{x_l}, k_{y_m})\exp\left(\frac{\mathrm{i}2\pi mj}{N_y}\right) \tag{5}$$

$$q(x_i, y_j) = \tilde{q}(0, y_j) + 2\sum_{l=1}^{N_x/2} \tilde{q}(k_{x_l}, y_j)\exp\left(\frac{\mathrm{i}2\pi li}{N_x}\right) \tag{6}$$

Chebyshev transformations are used for the wall-normal direction with the help of the Chebyshev polynomial $T_n(z_k)$[23]:

$$\tilde{q}_n = \sum_{k=0}^{N_z-1} q(z_k)T_n(z_k), \qquad q(z_k) = \sum_{n=0}^{N_z-1} \tilde{q}_n T_n(z_k) \tag{7}$$

Dealiasing via the "$\frac{3}{2}$ rule" has been applied whenever nonlinear quantities are required. Time advance is achieved with a third-order Runge–Kutta method for the convective term and the Crank–Nicolson method for the pressure and viscous terms. An implicit treatment is employed to avoid extremely small time steps in the near-wall region owing to the Chebyshev discretization. In all simulations the reference pressure is taken as the instantaneous upper wall pressure averaged over the periodic directions. The initial flowfields consist of an approximate mean turbulent flow with superimposed artificial disturbances. Statistical data are accumulated only after the initial influence has disappeared, and the flow has statistically settled down. Convergence is checked by comparing the statistical data in successive time segments, making sure that they are consistent. All statistical data are averaged over the horizontal plane and over time; averaged quantities are denoted by an overbar.

The parallel implementation of Sandham and Howard[21] is employed for all of the simulations. More details of the numerical method can be found in Refs. 21–23.

III. Validation of DNS

A. Plane Poiseuille Flow

To justify the application of periodic boundary conditions to fully developed turbulent channel flow, the computational domain must be large enough to include the largest eddies in the flow. Four test cases at $Re_\tau = 180$ were run with different boxes and resolutions before the final simulations were carried out. The box size was increased until both the streamwise and the spanwise two-point correlations dropped to zero at maximum separation (half the box size as a result of the periodic boundary condition).

The computational domain finally chosen is $24h^* \times 12h^* \times 2h^*$, which is approximately twice (in L_x and L_y) what was used in Kim, Moin, and Moser[3] (referred to as KMM hereafter). The velocity correlations, shown in Fig. 1 at the channel centerline, show that the two-point correlations fall to zero at large separation (maximum value 0.008 for the streamwise and 0.006 for the spanwise), demonstrating that the computational domain used is adequate. The total

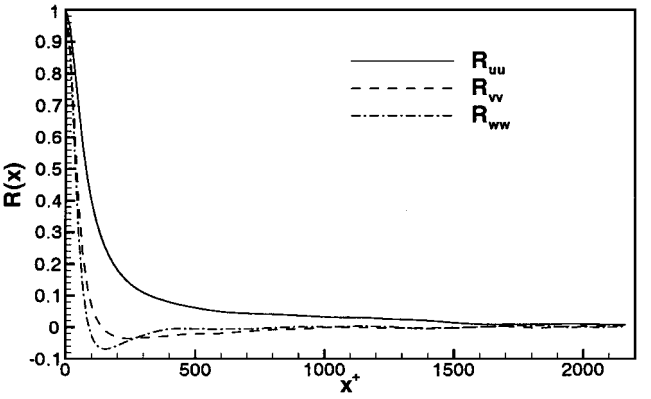

a) Streamwise

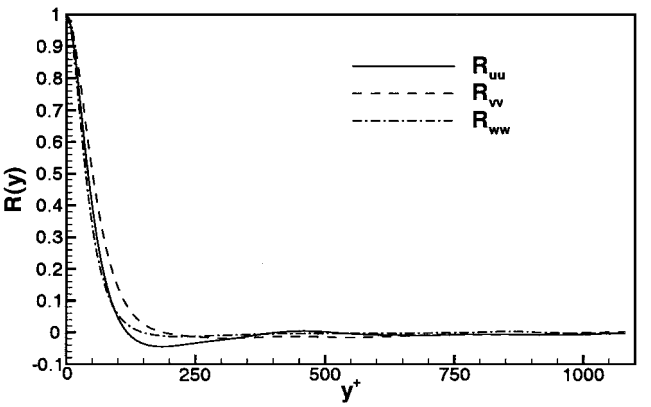

b) Spanwise

Fig. 1 Two-point velocity correlations of Poiseuille flow at channel centerline.

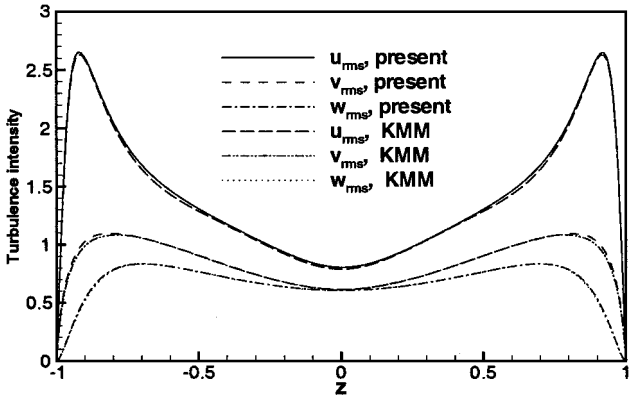

Fig. 2 Turbulence intensity [$u_{i_{\rm rms}} = \sqrt{(u_i^* u_i^*)}/u_\tau^*$] of Poiseuille flow.

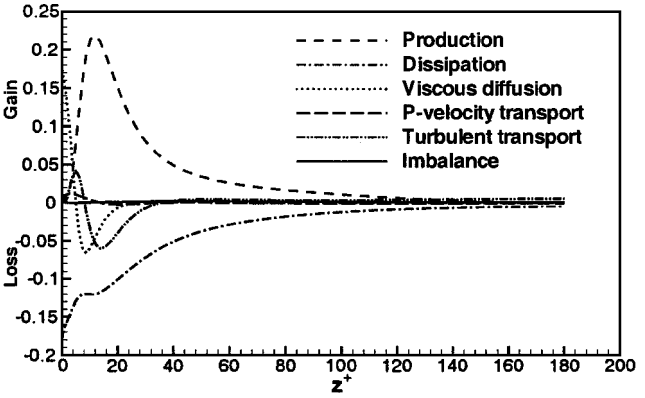

Fig. 3 Turbulent kinetic energy budget of Poiseuille flow.

number of grid points used is about 8 million ($256 \times 256 \times 121$ in x, y, z), with spacing of 16.88 and 8.44 wall units in the streamwise and spanwise direction, respectively, which is comparable to KMM. It was carried out with 64 processors on a Cray T3E and required about 16,000 processor element (PE) hours.

Figure 2 shows the Poiseuille flow turbulence intensities normalized by u_τ^*. Symmetry about the centerline for all results indicates well-converged statistics. The turbulence intensities are in good agreement with KMM (the thin lines are overlapped by the thick lines of the present results).

From the continuity and momentum equations we can derive the transport equation of the nondimensional turbulent kinetic energy $k = \frac{1}{2}\overline{u_i' u_i'}$ for plane channel flow as

$$\frac{\partial k}{\partial t} + \overline{u}_j \frac{\partial k}{\partial x_j} = -\overline{u_i' w'} \frac{\partial \overline{u}_i}{\partial z} - \overline{\tau_{ij}' \frac{\partial u_i'}{\partial x_j}} - \frac{\partial \overline{p' w'}}{\partial z} - \frac{\partial \left(\frac{1}{2}\overline{u_i' u_i' w'}\right)}{\partial z} + \frac{1}{Re}\frac{\partial^2}{\partial z^2}(k + \overline{w' w'}) \tag{8}$$

The terms on the right-hand side are the production, dissipation, pressure–velocity transport, turbulent transport, and viscous diffusion. After the flow has become statistically stable, the terms on the right-hand side should sum to zero.

A budget of the turbulent kinetic energy has been calculated as a check on our simulation results, as shown in Fig. 3. The budget imbalance (sum of all terms on the right-hand side) is more than two orders of magnitude smaller than the maximum production.

B. Plane Couette Flow

Four test cases at Reynolds number $Re_w = 1.3 \times 10^3$ were carried out, with different box sizes and resolutions, before the final simulation was performed in a computational domain of $192h^* \times 24h^* \times 2h^*$ with about 42.5 million grid points ($1024 \times 512 \times 81$ in x, y, z). The simulation was run with 128 processors on a Cray T3E, requiring about 15,000 PE hours. The grid spacing is 15.38 and 7.69 wall units in the streamwise and spanwise direction, respectively. The computational box is large enough to allow periodic

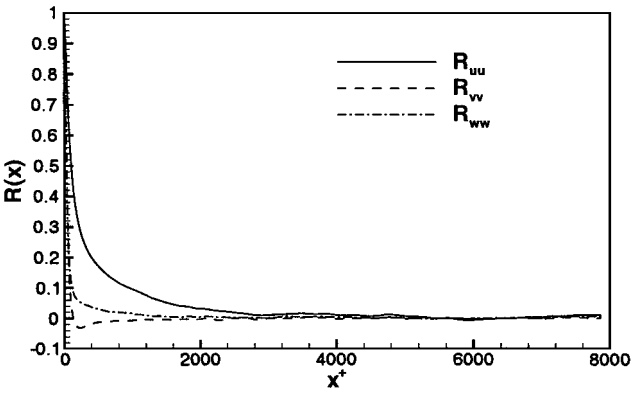

a) Streamwise

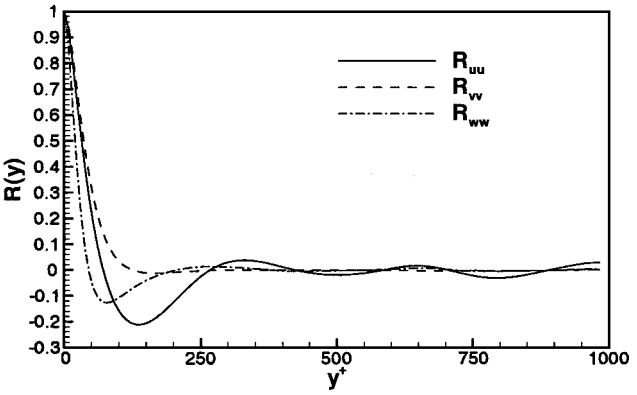

b) Spanwise

Fig. 4 Two-point velocity correlations of Couette flow at channel centerline.

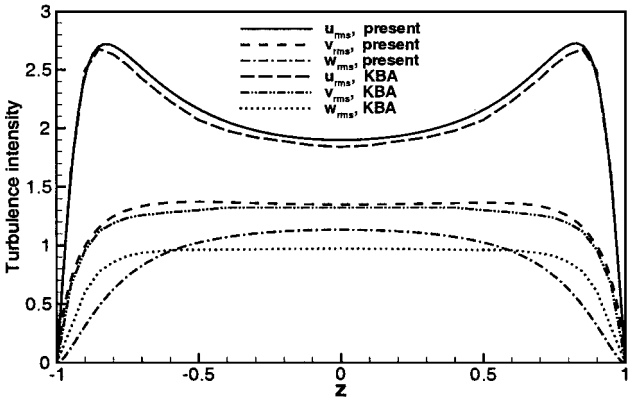

Fig. 5 Turbulence intensity [$u_{i_{\rm rms}} = \sqrt{(u_i^* u_i^*)}/u_\tau^*$] of Couette flow.

boundary conditions to be applied in both streamwise and spanwise directions, as demonstrated by the streamwise and spanwise two-point correlations shown in Fig. 4 for the channel centerline (the worst location).

Turbulence intensities for plane Couette flow are given in Fig. 5, with all quantities normalized by u_τ^*. Results of Kristoffersen, Bech, and Andersson[6] (referred to as KBA hereafter) are plotted with thin lines for comparison. The streamwise and spanwise turbulence intensities of KBA are close to our results in the near-wall region but smaller elsewhere; the differences are almost certainly caused by the coarser resolution and smaller box used in KBA. KBA used a second-order central finite difference method for all spatial derivatives and a second-order Adams–Bashforth scheme for time advance. The grid spacing used by KBA is 11.12 and 8.34 wall units for the streamwise and spanwise directions, respectively, compared to 15.38 and 7.69 for the present simulation. Although their Δx^+ is smaller, the effective resolution is still lower because of the higher accuracy of the present spectral method. The wall-normal resolution of KBA is also lower with only 64 points, compared with 81 points

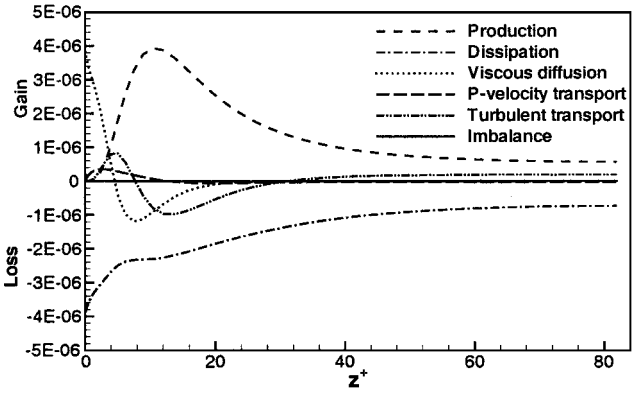

Fig. 6 Turbulent kinetic energy budget of Couette flow.

in the present simulation. Comparison between test cases with different resolutions shows that coarse resolution will give smaller turbulence intensities in the streamwise and spanwise directions. Another difference is that the computational box used in KBA is $4\pi h^* \times 2\pi h^* \times 2h^*$, which is not large enough to get two-point correlations dropping to zero, as shown in their two-point correlation results.

Figure 5 shows large differences exist in the wall-normal turbulence intensity, with the results of KBA being flat in the channel center. Komminaho et al.[8] ran a Couette flow simulation at $Re_w = 750$ in a box of $28\pi h^* \times 8\pi h^* \times 2h^*$, and their results for wall-normal turbulence intensity also show a similar profile with no flat region.

A budget of Couette flow turbulent kinetic energy is shown in Fig. 6. The budget balance is about three orders of magnitude smaller than the maximum production.

IV. Wall-Pressure Fluctuations

A. Wave-Number–Frequency Spectral Density of Wall Pressure

A continuous variable $q(x, y, t)$ defined over $0 \le x \le L_x$, $0 \le y \le L_y$, and $0 \le t \le T$, such as fluctuating pressure or shear stress on the wall, is represented in the DNS simulation by the sampled variable $q(x_i, y_j, t_r)$ with discrete Fourier transform $\tilde{q}(k_{x_l}, k_{y_m}, f_s)$. The transformation is performed using Eqs. (3) and (4), followed by the discrete time transform

$$\tilde{q}(k_{x_l}, k_{y_m}, f_s) = \frac{1}{N}\sum_{r=0}^{N-1} \tilde{q}(k_{x_l}, k_{y_m}, t_r)\exp\left(\frac{\mathrm{i}2\pi rs}{N}\right) \qquad (9)$$

Here t_r is the time of the sample given by $t_r = r\Delta t$, where Δt is the sampling interval, and f_s is the nondimensional frequency, $f_s = s/(\Delta t N)$, with $0 \le s \le N/2$ (r and s are integers).

The two-sided wave-number–frequency spectral density of q, $S_q(k_{x_l}, k_{y_m}, f_s)$, is defined as

$$S_q(k_{x_l}, k_{y_m}, f_s) = E\left\{\lim_{L_x, L_y, T \to \infty}\left[\frac{(2\pi)^{-2}}{L_x L_y T}\tilde{q}\tilde{q}^{\star}\right]\right\} \qquad (10)$$

The factor of $(2\pi)^{-2}$ comes from the use of wave-number components k_x, k_y rather than spatial frequencies. The sign convention used here for time Fourier transformation differs from the usual one. The time transform is defined so that waves with the same sign of streamwise wave number and frequency travel with the flow, and waves with opposite signs travel against the flow.

In the simulation the pressures on both channel walls were stored as a function of spatial wave number (k_x, k_y), every five time steps for Poiseuille flow and two time steps for Couette flow, after the flow had statistically settled down. Each (k_x, k_y) component was time Fourier transformed with Eq. (9), and the wave-number–frequency spectral density of wall pressure was then calculated by Eq. (10).

B. Plane Poiseuille Flow

Figure 7 shows the upper wall pressure for Poiseuille flow, expressed as wave-number–frequency spectral density at six positive

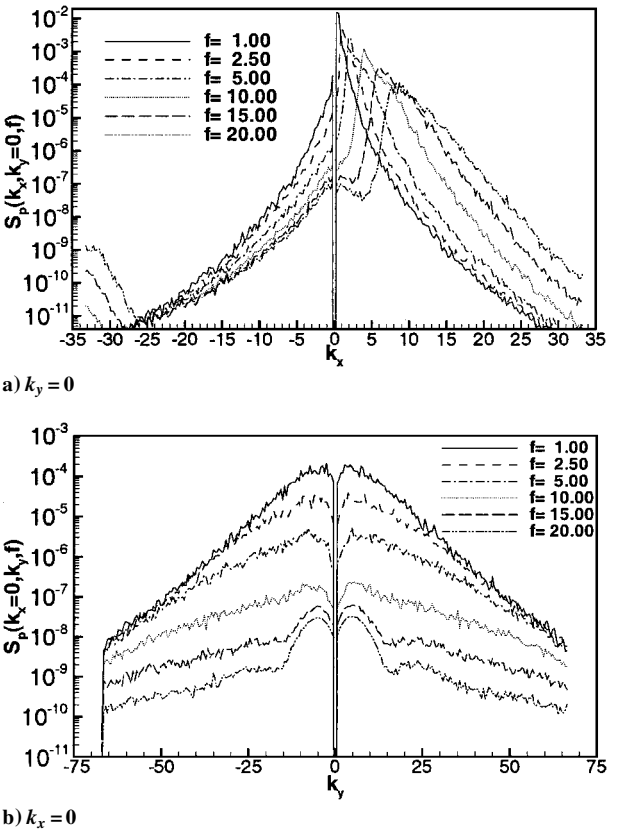

Fig. 7 Wave-number spectral density of Poiseuille flow upper-wall pressure. The small increase at high negative k_x in a) is a numerical artifact.

frequencies, at Reynolds number $Re_\tau = 180$. Wall scaling ($u^*_{\mathrm{ref}} = u^*_\tau$) is used throughout the presentation of Poiseuille flow results. The spectral density at positive streamwise wave numbers is generally much larger than at corresponding negative wave numbers, meaning that there is more energy in the forward moving waves. For the spanwise direction, as there is no mean flow and the flow is homogeneous in this direction, symmetry is found between negative and positive wave numbers.

In all of the simulations of plane channel flow, the mean wall pressure is used as the reference pressure at every time step, and so the calculated wall pressure spectral density is zero at $k_x = 0$, $k_y = 0$ for all frequencies. This explains the sudden drop of wall-pressure spectral density in Fig. 7 at zero wave number.

The spectral density of the lower-wall pressure is very similar to that of the upper wall, as is expected from the symmetry of plane Poiseuille flow.

1. *Low-Wave-Number Behavior*

Fluctuating wall pressures and wall shear stresses in the subconvective wave-number region have important implications for structural response.[15] The low-wave-number behavior of the fluctuating wall pressure under an incompressible turbulent boundary layer remains controversial, as discussed in the Introduction. On one hand, Chase[13] found that when the viscous no-slip wall boundary condition is applied the low-wave-number spectra of wall pressure and shear stress approach nonvanishing, "wavenumber-white" asymptotic limits. On the other hand, this prediction was contradicted by Howe,[15] who considered the normal force on a rigid strip, of finite width and infinite length, caused by a nearby vortical region in viscous flow. By taking the limit of large strip width, Howe calculated that the Kraichnan–Phillips theorem holds for homogeneous turbulent flow over an infinite plane wall, provided the flow is incompressible and free of other boundaries.

From the DNS results in Fig. 7, we can see that the wall-pressure spectral density is certainly finite at low wave number. With increasing frequency there is evidence for a broadening of the nearly flat region in Fig. 7a. In other words, the wall-pressure spectral density

has a tendency to become wave-number-white in the subconvective region (more apparent at the high frequencies), in agreement with the theoretical prediction of Chase[13] rather than Howe.[15]

The small increase in the wall-pressure spectral density at large negative k_x for high frequencies is an effect of numerical resolution. Numerical experiments have shown that higher resolution will give monotonically decreasing spectra.

2. Convective Peaks in the Wall-Pressure Spectrum

In Fig. 7a convective peaks in the streamwise wave-number spectrum can be seen, with the peak moving to higher wave numbers as the frequency is increased. The same phenomenon is shown in Fig. 8, where the frequency spectrum is plotted for different streamwise wave numbers. In both cases the spanwise wave number is set equal to zero. The peak frequency–wave-number combinations from the wave-number plot (Fig. 7a) and the frequency plot (Fig. 8) are plotted in Fig. 9, using triangles and squares, respectively. As expected, the peak wave number varies linearly with frequency. The wall-pressure convection velocity u_c calculated from $u_c = 2\pi f/k_x$ is equal to 14.91 (scaled on u_τ^*). The maximum velocity $u_{\max}$, which is the channel centerline velocity, is 18.20, and so the convection velocity $u_c = 0.819u_{\max}$. An equivalent statement, based on the nondimensional mean velocity u_m of 15.62, is $u_c = 0.955u_m$.

To study the influence of Reynolds number, simulations have been carried out for Reynolds numbers $Re_\tau = 90$, 180, and 360. The wall-pressure wave-number spectra are compared in Fig. 10 for $f = 15$. A convective peak exists for every Reynolds number, but the higher the Reynolds number the broader the wave-number spectrum.

The wall-pressure spectrum has been compared with experimental results of Brungart et al.[24] for channel flow, Lauchle and Daniels[25] for fully developed pipe flow, and Schewe[26] for an external boundary layer, as shown in Fig. 11. The point spectrum of wall pressure, $G_T^*(\omega)$ ($\omega = 2\pi f$), is calculated from the wave-number–frequency spectrum, based on the definition of Lauchle and Daniels.[25] The point spectra of the DNS results show a consistent

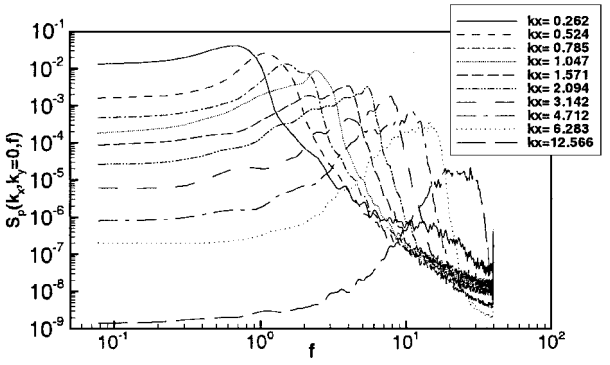

Fig. 8 Frequency spectral density of Poiseuille flow upper-wall pressure ($k_y = 0$).

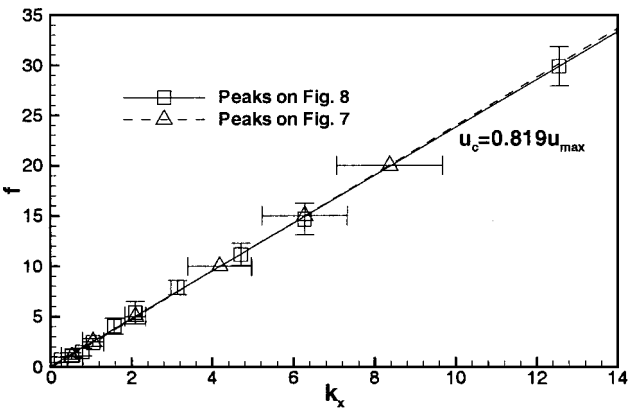

Fig. 9 Peak streamwise wave number of Poiseuille flow wall-pressure spectrum.

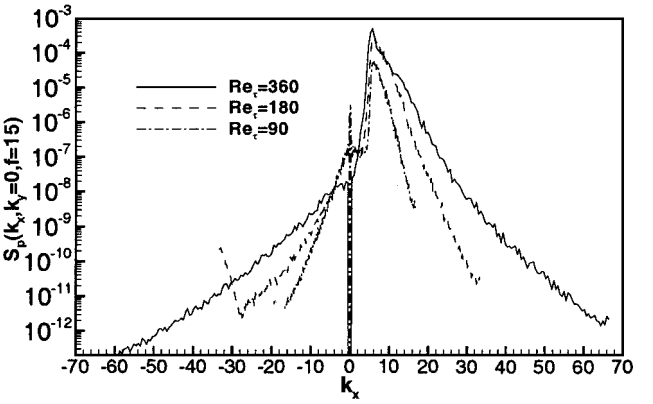

Fig. 10 Wave-number spectral density of wall pressure in Poiseuille flow for different Reynolds numbers ($k_y = 0$). Scaled frequency $f = 15$.

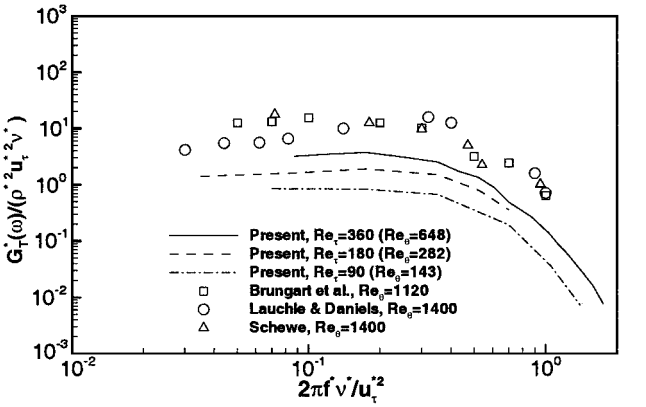

Fig. 11 Point spectrum of wall pressure in Poiseuille flow compared with experimental results.

trend with Reynolds number, approaching the experimental data as the Reynolds number is increased. It is possible to collapse the DNS data at different Reynolds numbers by plotting $G_T^*(\omega)/(\rho^{*2}u_{\max}^{*3}h^*)$ on the vertical axis.

C. Plane Couette Flow

Figure 12 shows the upper-wall pressure in plane Couette flow, expressed as wave-number–frequency spectral density $S_p(k_x, k_y, f)$ at six different frequencies, at a Reynolds number $Re_w = 1.3 \times 10^3$. The scaled frequency f in Couette flow is defined as $f = f^*h^*/u_w^*$, and the pressure and wall shear stresses are normalized by $(\rho^* u_w^{*2})$. Repeating Fig. 12a for the lower wall gives an antisymmetric result, which is consistent with the antisymmetric mean flow.

The sudden drop of wall-pressure spectral density at wave number (0, 0) is an artifact of the calculation, as just explained for Poiseuille flow. It is clear from Fig. 12 that the wall-pressure spectral density tends to a nonzero value as both wave-number components (k_x, k_y) approach zero, as in Poiseuille flow.

For any given frequency the wave-number spectral density of the wall pressure has a peak for waves travelling in the same direction as the wall, as shown in Fig. 12a. The streamwise wave numbers corresponding to the peak are plotted against frequency in Fig. 13; the wave number varies linearly with frequency. The convection velocity u_c^* is calculated as $0.528u_w^*$.

In Fig. 14 the wall-pressure spectrum is plotted as a function of frequency for fixed k_x and k_y. Unlike the corresponding plot for Poiseuille flow in Fig. 8, the spectra in Fig. 14 fall off monotonically with frequency. No points have therefore been added to Fig. 13.

To study the influence of Reynolds number, a further simulation at $Re_w = 3.4 \times 10^3$ was run. The wall-pressure spectra are compared in Fig. 15. Similar convective peaks are found for the two cases, but the height of the spectrum generally increases as Re_w is increased from 1.3×10^3 to 3.4×10^3.

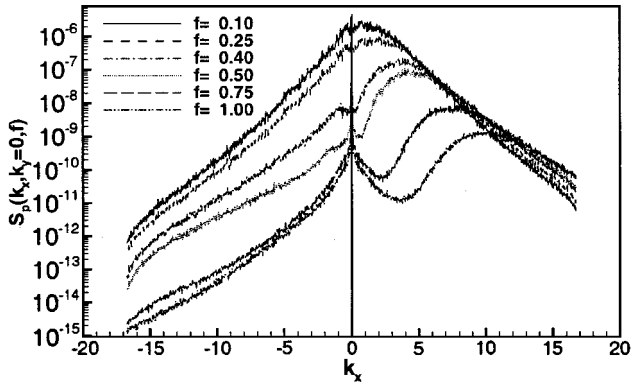

a) $k_y = 0$

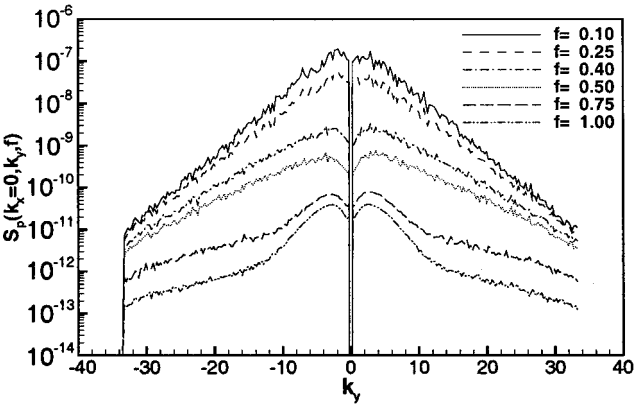

b) $k_x = 0$

Fig. 12 Wave-number spectral density of Couette flow upper-wall pressure.

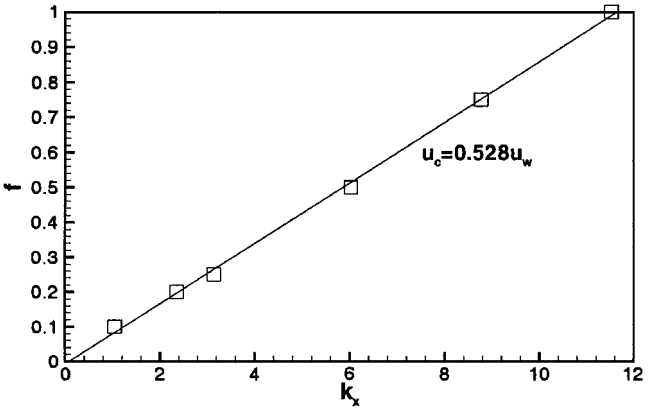

Fig. 13 Peak streamwise wavenumber of Couette flow wall-pressure spectrum.

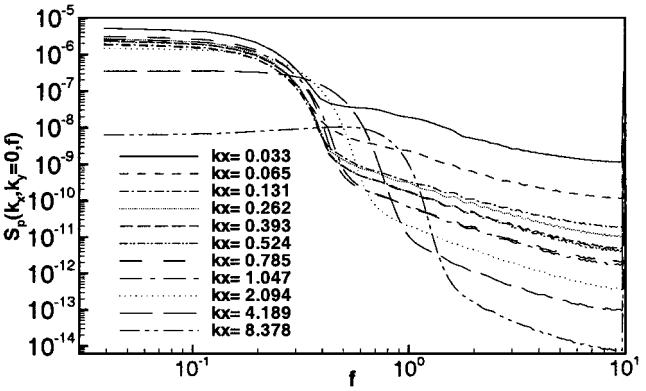

Fig. 14 Frequency spectral density of Couette flow upper-wall pressure ($k_y = 0$).

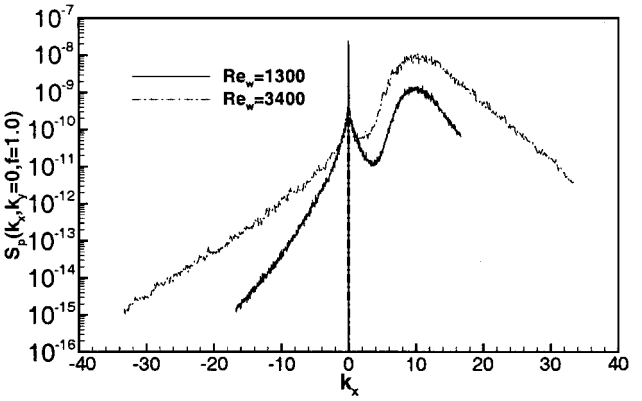

Fig. 15 Wall-pressure spectral density of Couette flow for different Reynolds numbers ($k_y = 0$).

V. Wall Shear-Stress Fluctuations

A. Wave-Number–Frequency Spectral Density of Wall Shear Stress

Plane channel flow has two wall shear-stress components, streamwise $(\tau_{xz})_w$ and spanwise $(\tau_{yz})_w$. Only the spectral density of $(\tau_{xz})_w$ is shown in this section. Results for the spectral density of $(\tau_{yz})_w$ show similar low-wave-number and convective properties. In the following discussion wall shear stress will refer to $(\tau_{xz})_w$ and will be denoted by τ_w for simplicity.

In the same way as for wall pressure, time series of wall shear stresses are saved in the DNS database as a function of (k_x, k_y), and the wave-number–frequency spectral density of wall shear stress is calculated from Eqs. (9) and (10).

B. Plane Poiseuille Flow

The theoretical studies of Chase[13,16,17] reached the conclusion that the shear stress on an infinite plane wall bounding an infinite incompressible flow also has a nonvanishing spectrum at vanishing wave number. Experimental data from Morrison et al.,[27] with an assumption of finite wall shear-stress spectra at zero wave number, led Chase to a semi-empirical model of the wave-number–frequency spectral density of streamwise turbulent wall shear stress.[17] Howe[20] also concluded that wall shear stress has a similar low-wave-number behavior to the wall pressure, but predicted zero spectral density at zero wave number.

1. *Low-Wave-Number Behavior*

Figure 16 shows the upper wall shear stress for Poiseuille flow, expressed as a wave-number–frequency spectral density at six scaled frequencies. In the subconvective region the wall shear-stress spectral density tends to be flatter at higher frequencies: the higher convective wave numbers at high frequency lead to a broader subconvective region. There is clearly a finite wall shear-stress spectral density in the low-wave-number limit.

2. *Convective Peaks in the Wall Shear-Stress Spectrum*

Figure 17 shows the frequency spectral density for upper-wall shear stress at different positive streamwise wave numbers. The wall shear-stress spectral density has a flat low-frequency region and then reaches a peak. These peaks, and the corresponding peaks found in the wave-number spectral density, are similar to the wall-pressure convective peaks discussed earlier. The peak frequency–wave-number combinations are plotted in Fig. 18. The convection velocity u_c calculated from the wave-number spectral peaks is 10.91, which is $0.599u_{\max}$. A slightly different value, $0.537u_{\max}$, is obtained from the peaks in the frequency spectra. Both values are smaller than the wall-pressure convection velocity for the same flow, which was $0.819u_{\max}$.

Our results for wall-pressure and wall shear-stress convection velocity, based on streamwise-wave-number spectral peaks at zero spanwise wave number, can be compared with the corresponding results from Jeon et al.[28] based on two-dimensional (k_x, f) spectra. Jeon et al.[28] found $u_c = (0.7 - 0.9)u_{\max}$ for p_w and $u_c = (0.55 - 0.8)u_{\max}$ for τ_w, whereas our results for $k_y = 0$ are $0.819u_{\max}$ and $0.537u_{\max}$, respectively.

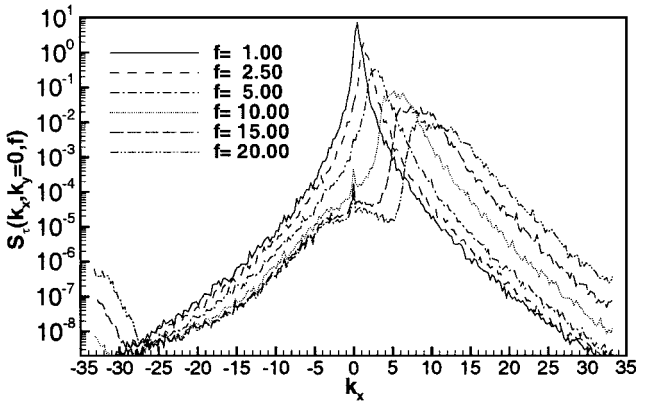

a) $k_y = 0$

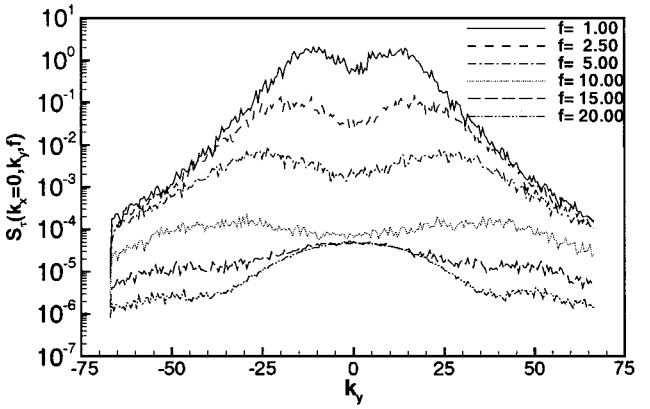

b) $k_x = 0$

Fig. 16 Wave-number spectral density of Poiseuille flow upper-wall shear stress.

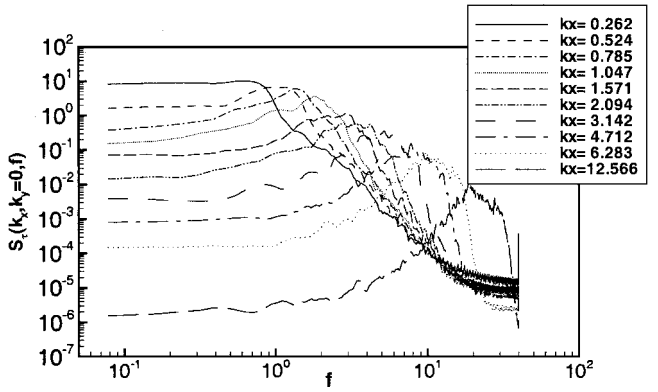

Fig. 17 Frequency spectral density of Poiseuille flow upper-wall shear stress ($k_y = 0$).

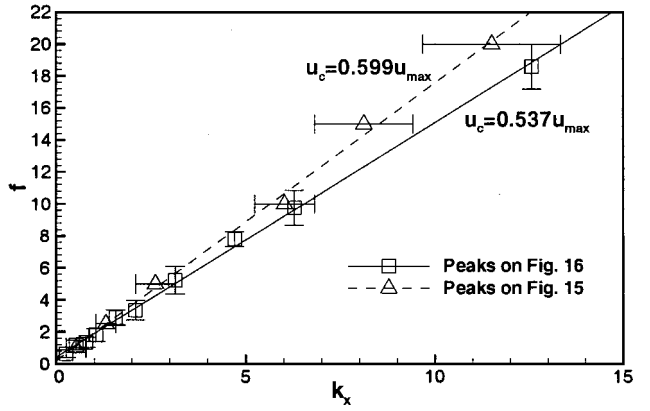

Fig. 18 Peak streamwise wave number of Poiseuille flow wall shear-stress spectrum.

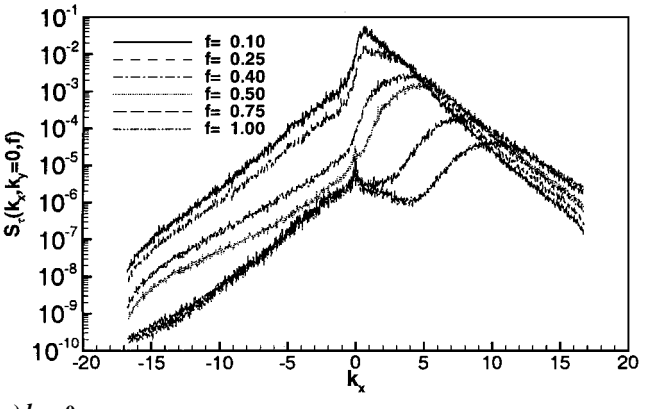

a) $k_y = 0$

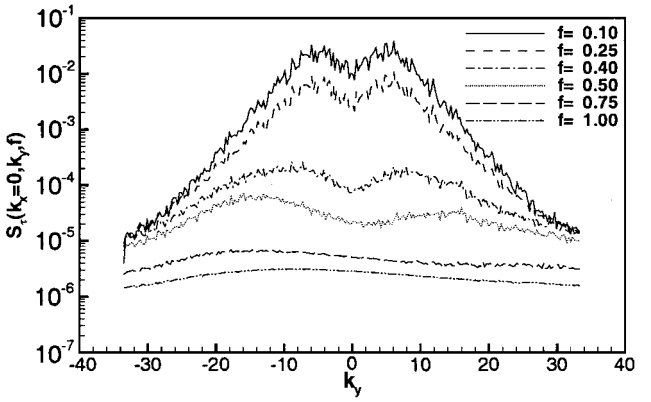

b) $k_x = 0$

Fig. 19 Wave-number spectral density of Couette flow upper-wall shear stress.

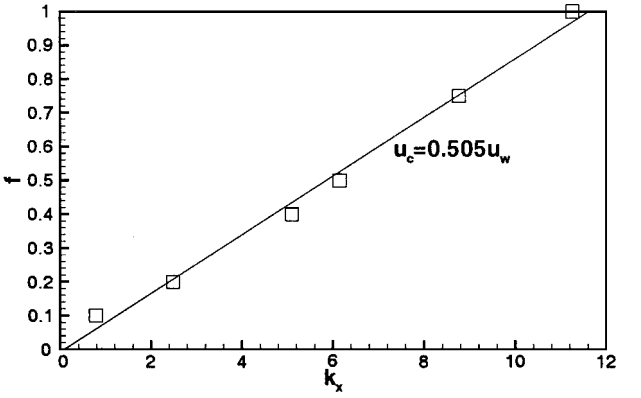

Fig. 20 Peak streamwise wave number of Couette flow wall shear-stress spectrum.

C. Plane Couette Flow

Figure 19 shows the upper-wall shear stress for plane Couette flow, expressed as a wave-number–frequency spectral density. The same plot for the lower wall, which moves with a negative wall velocity $-u_w^*$, is the mirror image of this.

As with the Poiseuille flow wall shear-stress spectra, there clearly exists a nonzero limit for the spectral density at low wave numbers.

The peaks from the wave-number spectrum plot in Fig. 19a are plotted for each frequency in Fig. 20. The convection velocity is equal to $0.505u_w^*$. The frequency spectral density of Couette wall shear stress is shown in Fig. 21.

VI. Consistency of Results

The wave-number–frequency spectral densities of wall pressure and shear stresses should not be influenced by the box size (L_x, L_y) and the record length (T). The consistency of the spectral density results with respect to variations in computational box size and T

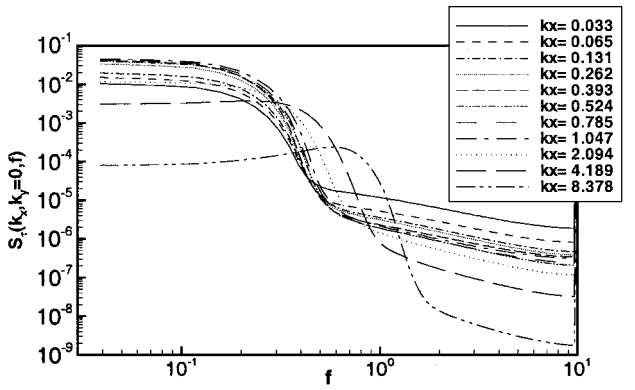

Fig. 21 Frequency spectral density of Couette flow upper-wall shear stress ($k_y = 0$).

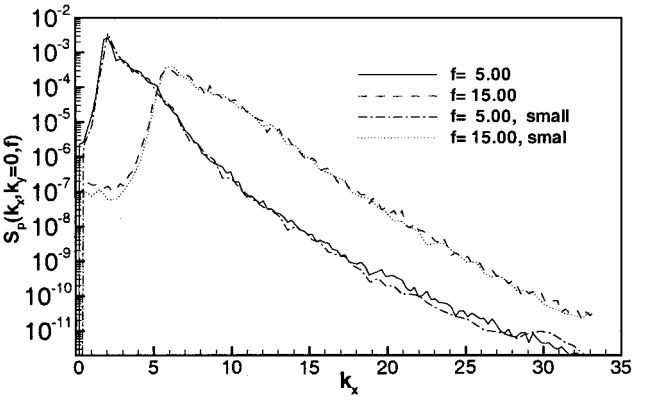

Fig. 22 Wave-number spectral density of upper-wall pressure in Poiseuille flow for different computational boxes.

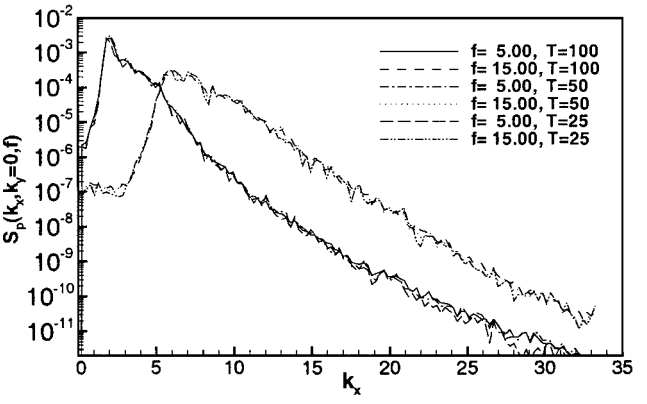

Fig. 23 Wave-number spectral density of upper-wall pressure in Poiseuille flow for different record lengths.

has been checked for each case. Figure 22 shows the wall-pressure spectral density results for Poiseuille flow, compared with data from a small computational box of $12h^* \times 6h^* \times 2h^*$ (labeled as "small"), which is half the final computational box size in both the streamwise and spanwise directions. The results are consistent for different box sizes, indicating that the computational domain is large enough. Enlarging the computational box improves the low-wave-number resolution with more modes in the subconvective region, making the low-wave-number behavior of wall-pressure spectral density clearer in the subconvective wave-number region.

A check on record length has also been done for each case, as shown in Fig. 23 for the Poiseuille flow wall-pressure spectral density. Results for different times $T = 100, 50$, and 25 collapse for both $f = 5$ and 15. The agreement shows our results are not influenced by record length limitations.

Results from different box sizes and record lengths agree to within 3 dB. Larger computational boxes and longer record lengths give smoother spectra.

VII. Conclusions

Plane Poiseuille and Couette flow have been simulated in very large computational domains, sufficient to ensure that the two-point velocity and pressure correlations drop to zero in both streamwise and spanwise directions. The present results have been compared with existing data, and good agreement has been found. Direct numerical simulation databases have been set up for the wall pressure and shear stress to study their wave-number–frequency spectral densities. The spectral density of wall pressure and shear stress both exhibit a nonzero low-wave-number limit in the subconvective region. This is consistent with Chase's[13] theoretical study for flow over a single wall but contradicts Howe.[15] The wall-pressure and shear-stress spectra are, however, very similar to each other, as predicted by both authors.[13,19,20] Convective peaks are found in the wave-number spectra of wall pressure and shear stress: for Poiseuille flow the convection velocity of wall pressure is 35–40% larger than that of wall shear stress, whereas for Couette flow it is only 5% larger.

Acknowledgments

This study is supported by the Engineering and Physical Sciences Research Council (EPSRC) under Grant GR/M38865, and the Cray T3E time is provided by EPSRC Grant GR/M08424.

References

[1]Hussain, A. K. M. F., and Reynolds, W. C., "Measurements in Fully Developed Turbulent Channel Flow," *Journal of Fluids Engineering*, Vol. 97, No. 3, 1975, pp. 568–578.

[2]Tillmark, N., and Alfredsson, P. H., "Experiments on Transition in Plane Couette Flow," *Journal of Fluid Mechanics*, Vol. 235, 1992, pp. 89–102.

[3]Kim, J., Moin, P., and Moser, R., "Turbulence Statistics in Fully Developed Channel Flow at Low Reynolds Number," *Journal of Fluid Mechanics*, Vol. 177, 1987, pp. 133–166.

[4]Mansour, N. N., Kim, J., and Mion, P., "Reynolds-Stress and Dissipation-Rate Budgets in a Turbulent Channel Flow," *Journal of Fluid Mechanics*, Vol. 194, 1988, pp. 15–44.

[5]Moser, R. D., Kim, J., and Mansour, N. N., "Direct Numerical Simulation of Turbulent Channel Flow up to $Re_\tau = 590$," *Physics of Fluids*, Vol. 11, No. 4, 1999, pp. 943–945.

[6]Kristoffersen, R., Bech, K. H., and Andersson, H. I., "Numerical Study of Turbulent Plane Couette Flow at Low Reynolds Number," *Applied Scientific Research*, Vol. 51, 1993, pp. 337–343.

[7]Hamilton, J. M., Kim, J., and Waleffe, F., "Regeneration Mechanisms of Near-Wall Turbulence Structures," *Journal of Fluid Mechanics*, Vol. 287, 1995, pp. 317–348.

[8]Komminaho, J., Lundbladh, A., and Johansson, A., "Very Large Structure in Plane Turbulent Couette Flow," *Journal of Fluid Mechanics*, Vol. 320, 1996, pp. 259–285.

[9]Kraichnan, R. H., "Pressure Fluctuations in Turbulent Flow over a Flat Plate," *Journal of the Acoustical Society of America*, Vol. 28, No. 3, 1956, pp. 378–390.

[10]Phillips, O. M., "On the Aerodynamic Surface Sound from a Plane Turbulent Boundary Layer," *Proceedings of the Royal Society of London, A*, Vol. 234, No. 1198, 1956, pp. 327–335.

[11]Chase, D. M., "Modeling the Wavevector–Frequency Spectrum of Turbulent Boundary Layer Wall Pressure," *Journal of Sound and Vibration*, Vol. 70, No. 1, 1980, pp. 29–67.

[12]Chase, D. M., "The Character of the Turbulent Wall Pressure Spectrum at Subconvective Wavenumbers and a Suggested Comprehensive Model," *Journal of Sound and Vibration*, Vol. 112, No. 1, 1987, pp. 125–147.

[13]Chase, D. M., "Fluctuations in Wall-Shear Stress and Pressure at Low Streamwise Wavenumbers in Turbulent Boundary-Layer Flow," *Journal of Fluid Mechanics*, Vol. 225, 1991, pp. 545–555.

[14]Herbert, K., Leehey, P., and Hai-Hariri, H., "On the Mach- and Reynolds- Number Dependence of the Flat-Plate Turbulent Boundary Layer Wall-Pressure Spectrum," *Theoretical and Computational Fluid Dynamics*, Vol. 13, 1999, pp. 33–56.

[15]Howe, M. S., "A Note on the Kraichnan–Phillips Theorem," *Journal of Fluid Mechanics*, Vol. 234, 1992, pp. 443–448.

[16]Chase, D. M., "Fluctuating Wall-Shear Stress and Pressure at Low Streamwise Wavenumbers in Turbulent Boundary-Layer Flow," *Journal of Fluids and Structures*, Vol. 6, No. 4, 1992, pp. 395–413.

[17]Chase, D. M., "A Semi-Empirical Model for the Wavevector–Frequency Spectrum of Turbulent Wall-Shear Stress," *Journal of Fluids and Structures*, Vol. 7, No. 6, 1993, pp. 639–659.

[18]Howe, M. S., "The Interaction of Sound with Low Mach Number Wall Turbulence, with Application to Sound Propagation in Turbulent Pipe Flow," *Journal of Fluid Mechanics*, Vol. 94, 1979, pp. 729–744.

[19]Howe, M. S., "The Role of Surface Shear Stress Fluctuations in the Generation of Boundary Layer Noise," *Journal of Sound and Vibration*, Vol. 65, No. 2, 1979, pp. 159–164.

[20]Howe, M. S., "The Damping of Sound by Wall Turbulent Shear Layers," *Journal of the Acoustical Society of America*, Vol. 98, No. 3, 1995, pp. 1723–1730.

[21]Sandham, N. D., and Howard, R. J. A., "Direct Simulation of Turbulence Using Massively Parallel Computers," *Parallel Computational Fluid Dynamics*, edited by D. R. Emerson, A. Ecer, J. Periaux, N. Satofuka, and P. Fox, Elsevier, Amsterdam, 1998, pp. 23–32.

[22]Kleiser, L., and Schumann, U., "Treatment of Incompressibility and Boundary Layer Conditions in 3D Numerical Spectral Simulations of Plane Channel Flows," *Proceeding of 3rd GAMM Conference on Numerical Method in Fluid Mechanics*, edited by E. H. Hirschel, Vieweg, Brunswick, Germany, 1980, pp. 165–173.

[23]Canuto, C., Hussaini, M. Y., Quarteroni, A., and Zang, T. A., *Spectral Methods in Fluid Dynamics,* Springer-Verlag, New York, 1987, pp. 216–219.

[24]Brungart, T. A., Lauchle, G. C., Deutsch, S., and Riggs, E. T., "Outer-Flow Effects on Turbulent Boundary Layer Wall Pressure Fluctuations," *Journal of the Acoustical Society of America*, Vol. 105, No. 4, 1999, pp. 2097–2106.

[25]Lauchle, G. C., and Daniels, M. A., "Wall Pressure Fluctuations in Turbulent Pipe Flow," *Physics of Fluids*, Vol. 30, No. 10, 1987, pp. 3019–3024.

[26]Schewe, G., "On the Structure and Resolution of Wall-Pressure Fluctuations Associated with Turbulent Boundary-Layer Flow," *Journal of Fluid Mechanics*, Vol. 134, 1983, pp. 311–328.

[27]Morrison, W. R. B., Bullock, K. J., and Kronauer, R. E., "Experimental Evidence of Waves in the Sublayer," *Journal of Fluid Mechanics*, Vol. 47, 1971, pp. 639–656.

[28]Jeon, S., Choi, H., Yoo, J. Y., and Moin, P., "Space-Time Characteristics of the Wall Shear-Stress Fluctuations in a Low-Reynolds-Number Channel Flow," *Physics of Fluids*, Vol. 11, No. 10, 1999, pp. 3084–3094.

P. J. Morris
Associate Editor